CrossMark

ORIGINAL PAPER

Analysis of the nonlinear dynamics of inter-cycle combustion variations in an ethanol fumigation-diesel dual-fuel engine

Li-Ping Yang · **Timothy A. Bodisco** ·
Ali Zare · **Norbert Marwan** · **Thuy Chu-Van** ·
Richard J. Brown

Abstract The nonlinear dynamics of a combustion system in a modern common-rail dual-fuel engine has been studied. Using nonlinear dynamic data analysis (phase space reconstruction, recurrence plots, recurrence qualification analysis and wavelet analysis), the effect of ethanol fumigation on the dynamic behaviour of a combustion system has been examined at an engine speed of 2000 rpm with engine load rates of 50%, 75% and 100% and ethanol substitutions up to 40% (by energy) in 10% increments for each engine load. The results show that the introduction of ethanol has a significant effect on inter-cycle combustion variation (ICV) and the dynamics of the combustion system for all of the studied engine loads. For pure diesel mode and lower ethanol substitutions, the ICV mainly exhibits multiscale dynamics: strongly periodic and/or intermittent fluctuations. As the ethanol substitution is increased, the combustion process gradually transfers to more persistent low-frequency variations. At different engine loads, we can observe the bands with the strongest spectral power density that persist over the entire 4000 engine cycles. Compared to high engine loads (75% and 100%), the dynamics of the combustion system at a medium engine load (50%) was more sensitive to the introduction of ethanol. At higher ethanol substitutions, the increased ICV and the complexity of the combustion system at the medium load are attributable to the enhanced cooling caused by the excessive ethanol evaporation, while the low-frequency large-scale combustion fluctuations for the higher engine loads are likely caused by cyclic excitation oscillation during the transition of the combustion mode.

L.-P. Yang (✉)
Institute of Power and Energy Engineering, Harbin
Engineering University, No. 145-1, Nantong Street,
Nangang District, Harbin 150001, China
e-mail: yangliping302@hrbeu.edu.cn

L.-P. Yang · A. Zare · T. Chu-Van · R. J. Brown
Biofuel Engine Research Facility, Queensland University
of Technology, Brisbane, QLD 4001, Australia

T. A. Bodisco
Faculty of Science, Engineering and Built Environment,
Deakin University, Geelong, VIC 3220, Australia

N. Marwan
Potsdam Institute for Climate Impact Research, 14412 Potsdam,
Germany

1 Introduction

Ethanol is a promising renewable energy source that has had significant attention in the literature over the previous decade [1–10]. In addition to being easily produced from a wide range of feedstock [11], its production cost is relatively low [1]. The combustion of ethanol in an internal combustion engine can produce higher thermal efficiency, compared to diesel fuel [11], in addition to lower CO_2, NOx and PM emissions [3,12]. Because of

these reasons, ethanol is a serious contender to mitigate fossil fuel usage. Although ethanol has been previously investigated as a potential fuel for internal combustion engines, interest in it was significantly reinvigorated in the 1970s as a consequence of the oil crisis [3,4].

Dual-fuel technology, utilising ethanol as the secondary fuel, has been recognised as an effective method to attain improved engine performance [5–10]. In dual-fuel operation, ethanol can be directly injected into the engine intake air upstream [13–15]. This method permits a substantial amount of ethanol to offset diesel fuel usage, without sacrificing the engine's performance; the maximum percentage of diesel energy replaced by ethanol has been shown to be as high as 60% [11,12]. In dual-fuel operation, no emulsion additives are required for stabilising the miscibility of ethanol and diesel as they are injected separately [16–18]. However, an extra fuel injection system is required: a second port injector, separate lines, pumps, fuel tanks and controls for the secondary fuel [19]. Compared to the blended mode, the fumigation method is more flexible; the engine operating mode could easily switch from dual-fuel to neat diesel fuel operation to suit the immediate mode of operation [1]. Similarly, the amount of diesel displaced by ethanol could be varied depending on the engine operation. A thorough understanding of the effect of ethanol fumigation is therefore required for the future development of sophisticated control systems.

The effects of ethanol fumigation on the performance of dual-fuel engines have been widely studied [5–25]. It is well established in the literature that ethanol fumigation can improve thermal efficiency while decreasing NOx and soot emissions simultaneously at some engine operating conditions. However, at low load, HC and CO emissions increase, and improper addition of ethanol may cause substantially increased inter-cycle combustion variation (ICV) [23,24]. ICV leads to harmful fluctuations of the power output and increased toxic emissions. If ICV can be eliminated, engine power output has the potential to increase by 10%, for the same fuel consumption [26]. Therefore, understanding the characteristics of ICV and identifying contributing sources is important for further improvement in engine efficiency and emissions.

In most previous studies, utilising normal linear statistics on a time-averaged basis, the statistical aspects of ICV were characterised to give insight into the parametric effects on ICV and the linear dynamic features [27]. Only a few studies were conducted to correlate combustion quality from one engine cycle to the next based on time series analysis [28,29]. The predominant understanding of cyclic variability was that ICV was inherently either stochastic or deterministic in nature [26,30,31], and any determinism has been typically characterised in strictly linear terms [32]. However, recent research has shown that ICV is an inherent consequence of nonlinear combustion kinetics and highly chaotic behaviour will occur if the burn time occupies an excessive fraction of the cycle time [33].

Recently, nonlinear dynamical theory and data analysis approaches, based on time series analysis, have been rapidly developed to analyse the complex nonlinear dynamical systems. This approach has been increasingly applied to investigate the dynamic behaviours of combustions processes [34,35] and to assess system health [36], especially the ICV in internal combustion engines (ICE), for example, Poincaré maps, phase space reconstruction, recurrence plots (RPs), recurrence quantitative analysis (RQA) and wavelet transforms [27,32,36–45,47–49]. These approaches are particularly useful for revealing the geometric characteristics of combustion attractors and the temporal correlations between continuous engine combustion cycles in high -dimensional phase space and to discern the system complexity, transient and intermittent phenomena of ICV [50–55].

Historically, investigations into ICV have focused on spark ignition (SI) engines [37–47]; this is because compared to SI engines, the ICV from compression ignition (CI) engines is smaller. However, with increasingly strict regulations governing fuel efficiency and emissions, recent studies have directed their attention to compression ignition (CI) engines [48–51,56]. To date, however, there has not been any study performed to reveal the nonlinear dynamics of the combustion system in an ethanol-fumigated dual-fuel engine. In this regard, this study aims to experimentally examine the effect of ethanol fumigation on ICV in a modern common-rail dual-fuel engine and to systematically reveal the internal nature and complexity of the combustion system using return maps, RP, RQA and wavelet analysis and then identify the transition of the combustion mode and its correlation with dynamic complexities of the combustion system. Our research may be useful to understand the generation mechanism and the complex dynamic behaviour associated with combustion fluctuations and to promote the application of ethanol-fumigated dual-fuel engines.

Table 1 Engine specifications

Engine	Cummins
Number of cylinders	6
Fuel system	Common-rail
Intake system	Turbo-charged, inter-cooled
Bore × stroke	102 mm × 120 mm
Displacement	5.9 L
Compression ratio	17.3:1
Number of valves per cylinder	4
Maximum power/speed	162 kW/2500 rpm
Maximum torque/speed	820 Nm/1500 rpm

2 Facilities and experiment

The studied engine is a modified modern turbo-charged, common-rail diesel engine. The detailed specifications of the engine are shown in Table 1. A separate ethanol supply system was designed, which includes an ethanol tank, pump, filter, flowmeter, injector and pipes. The injector was mounted between the turbocharger and the inter-cooler on the inlet manifold. Ethanol injection was controlled by a separate electronic control unit (ECU). The engine load and speed were controlled by an electronically controlled hydraulic dynamometer. The schematic of the experimental bench is shown in Fig. 1.

Experiments were conducted at 2000 rpm with engine load rates of 50%, 75% and 100% of full load. For each engine load rate, the ethanol substitutions were performed by stabilising the engine at the required load and then reducing the engine load and directly introducing fumigated ethanol into the inlet manifold during the intake stroke until the original engine load was achieved. In order to keep a constant flow characteristic, the difference in pressure between the ethanol fuel rail and the post turbocharger manifold pressure was monitored and used as feedback to the ethanol pressure relief valve. The ethanol fumigation substitutions range from 0 to 40%, nominally at 10% intervals. The mass flow rates of diesel and ethanol were measured using an ethanol and a diesel flowmeter, respectively. The in-cylinder pressure was sampled using a piezo-electric pressure transducer and a DT9832 simultaneous analogue-to-digital converter (ADC). Crank angle (CA) and top dead centre (TDC) signals were acquired using a Kistler 2614 encoder into the same ADC. The sampling resolution of the crank angle signal was 0.5° of crank angle. But by means of interpolation between the known points, the limit of the crank angle resolution was improved to 0.06° CA at 2000 rpm, based on a sampling frequency of 200 kHz. For each test, the engine was allowed to run for a few minutes before the data were recorded. Each studied in-cylinder pressure data file contains 4000 engine cycles.

3 Analysis methods

The indicated mean effective pressure (IMEP) was calculated based on in-cylinder pressure and cylinder volume data (derived from the crank angle data), and the IMEP time series was used to perform phase space reconstruction and to calculate RPs, RQA measures and wavelet power spectra (WPS) to reveal the complex dynamic behaviour of the combustion system in an ethanol fumigation dual-fuel engine.

3.1 Phase space reconstruction

Phase space reconstruction was used to analyse the attractor's structure properties of the combustion system of an ethanol–diesel dual-fuel engine based on the IMEP time series $x(i)$, $(i = 1, 2, \ldots, N)$. The time-delay reconstruction was used to provide a set of m-dimensional vectors:

$$\mathbf{X}_i = \{x(i), x(i + \tau), \ldots, x(i + (m - 1)\tau\},$$
$$i = 1, 2, \ldots, N - (m - 1)\tau \qquad (1)$$

where $x(i)$ is the IMEP time series, $\mathbf{X}_i$ is the corresponding phase space vector, N is the number of samples, m is the embedding dimension, and τ is the time delay. In this study, the false nearest neighbours [57] and the mutual information function algorithms [58] were adopted to determine the optimum m and τ, respectively

3.2 Recurrence plot (RP)

As a graphical tool, the RP was introduced by Eckmann et al. [59]. Recurrence plots can be used to visualise the recurrences of dynamical systems [57,58]. An RP provides a qualitative analysis of the recurrence behaviour of a dynamic system. Usually, a high -dimensional
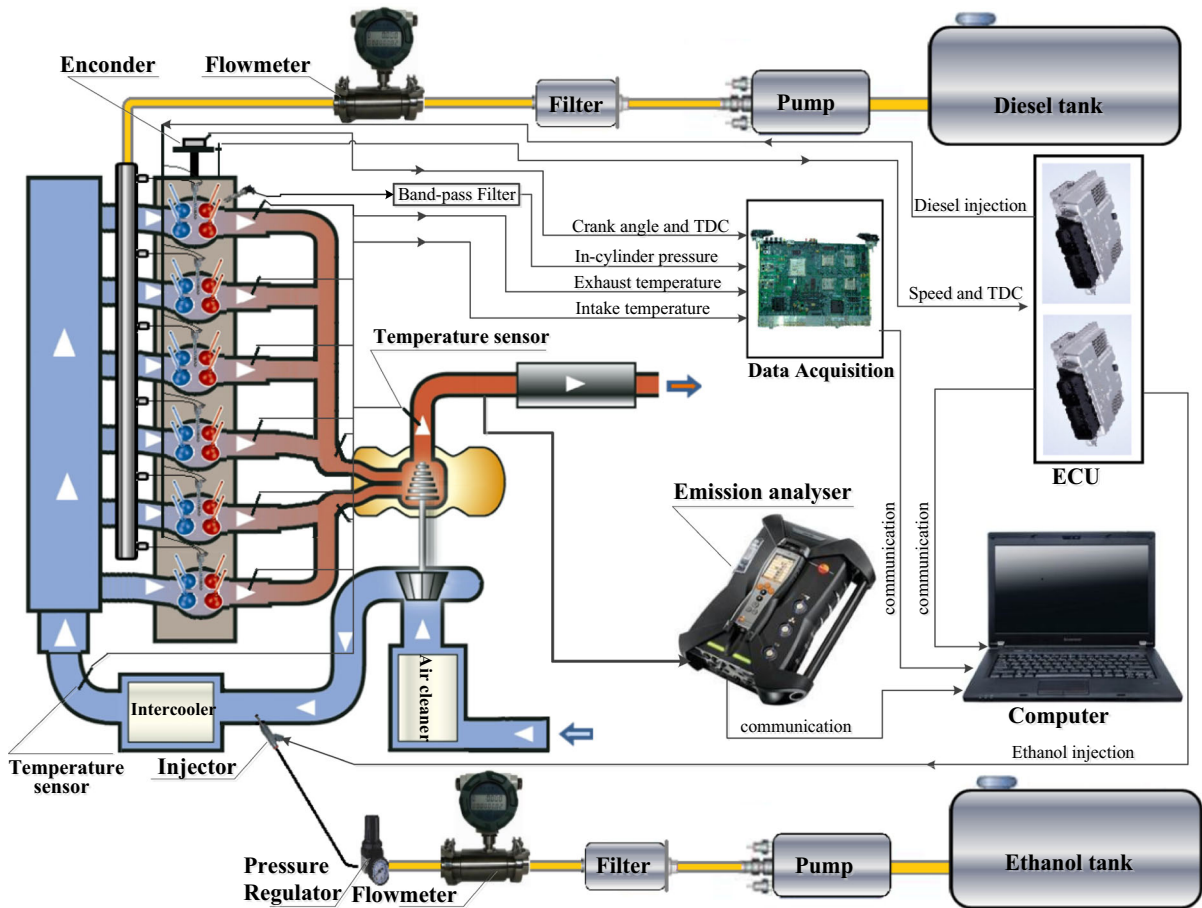
Fig. 1 Schematic of the experimental bench

phase space can only be visualised by projection into two- or three-dimensional subspace. The RP with characteristic small- and large-scale patterns makes it possible to reveal the dynamic characteristics of the trajectory motion in an m-dimensional phase space by using a two-dimensional representation of its recurrences. An RP is expressed as [60]:

$$R_{i,j} = \Theta\left(\varepsilon - \left\|\mathbf{X}_i - \mathbf{X}_j\right\|\right), \qquad (2)$$

where $\mathbf{X}_i$ and $\mathbf{X}_j$ are i-th and j-th points of the state space trajectory, $\|\cdot\|$ is the Euclidian norm, ε is the recurrence threshold, and $\Theta(s)$ is the Heaviside function, which is defined as:

$$\Theta(s) = \begin{cases} 1 & s \geq 0 \\ 0 & s < 0 \end{cases} \qquad (3)$$

The RP is a symmetric and square array of 1s and 0s. If the distances of point pairs $(\mathbf{X}_i, \mathbf{X}_j)$ at the reconstructed phase space trajectory are smaller than the recurrence threshold ε, the values of $R_{i,j}$ are 1. They are considered as recurrences and displayed using black. Otherwise, the values of $R_{i,j}$ are zero and displayed using white. The patterns in a RP are caused by typical dynamical behaviour and can be used to reveal temporal correlations. The information contained in a RP is rich and manifold and often cannot be easily obtained by other methods. Typical patterns in RPs can be linked to a specific behaviour of the dynamical system [60]. For example, RPs of stationary systems are homogeneous; long diagonal lines in the RP indicate periods of similar dynamics and can be hint of determinism in the system; periodically appearing patterns (such as long lines) are typical for periodic dynamics; block structures indicate intermittent dynamics; paling towards the corners
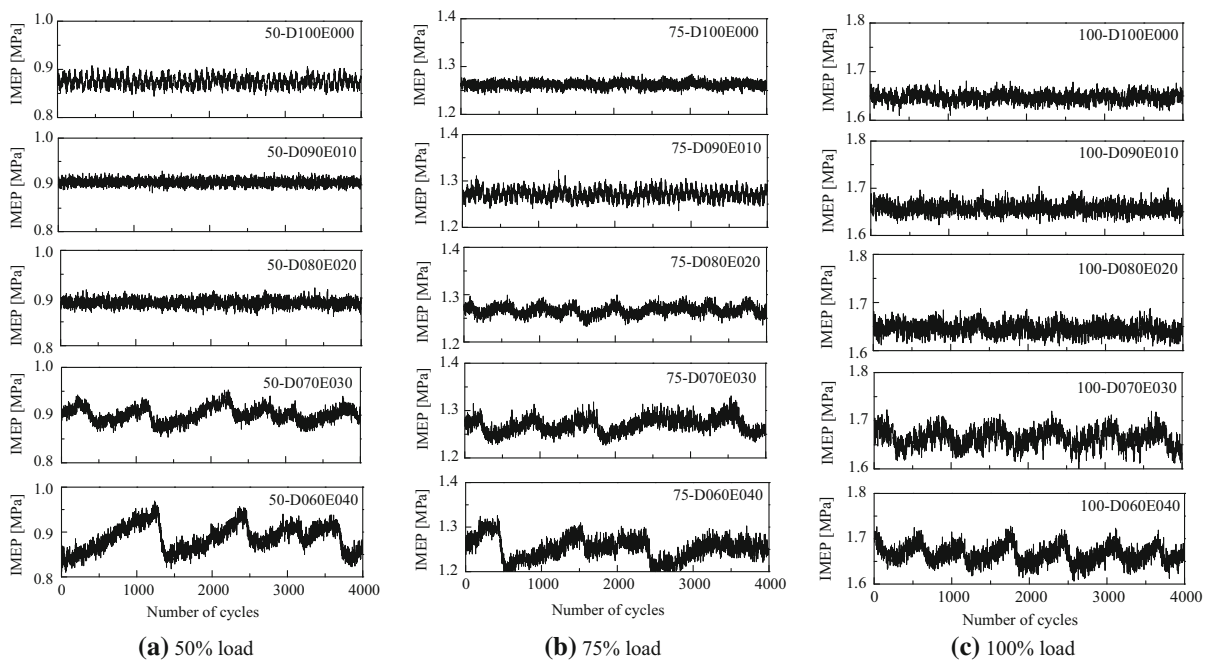
Fig. 2 IMEP time series when ethanol substitution is from 0 to 40% at different load rates of 50%, 75% and 100%

($i = 0$; $j = \max$) or ($i = \max$; $j = 0$) is signature of trend; white areas or bands in the RP indicate abrupt changes in the dynamics and extreme events; a lack of diagonal lines and appearance of single points occur for stochastic dynamics, etc.

The recurrence threshold ε has to be selected as a trade-off in such a way that there are still enough recurrences identified, but still small enough that obviously different states remain non-recurrent. Therefore, special attention needs to be paid to the choice of ε. In order to obtain reliable statistics in the RQA, the chosen threshold should be a trade-off between a required "as small as possible" threshold and a minimum number of recurrences. Several "rules of thumb" for the choice of ε have been suggested based on the maximum phase space diameter, standard deviation of the observational signal and recurrence point density of the RP [61–65]. Here, we have chosen a threshold that preserves the recurrence rate RR (Eq. 4) constant for all different experiment settings allowing for a better comparability of the results between the different settings and taking into account the amplitude differences (Fig. 2). A recurrence point density of 10% ensures a sufficient number of recurrence structures in the RP. Therefore, ε is selected that the recurrence rate is equal to 0.1 for the entire examined engine operating conditions. The values of m, τ and ε for different ethanol substitutions at various engine operating conditions are shown in Table 2.

3.3 Recurrence quantification analysis

The RP is an effective tool to get insights into the time evolution of the phase space trajectories; however, it can only provide a qualitative analysis of the recurrence behaviour of a dynamical system. RQA can go beyond the visual impression yielded by RPs and provide quantitative data, by quantifying the small-scale structures in RPs. Doing this can provide useful information even for non-stationary or shorter data when other analysis methods fail, such as identifying laminar states or detecting transitions between regular or chaotic regimes in complex systems [60,61]. Some RQA measures based on diagonal and vertical lines were calculated to reveal the complexity of the combustion system of an ethanol-diesel dual-fuel engine, such as the recurrence rate (RR), determinism (DET), line length entropy (ENTR), laminarity (LAM) and trapping time (TT) [60,61].

RR is a measure quantifying the recurrence density of a RP. It is an estimation of the recurrence probability of the system,

Table 2 Values of m, τ and ε

Engine load rate (%)	Ethanol substitution (%)	m	τ	ε
50	0	6	2	0.012
	10	6	3	0.009
	20	6	2	0.011
	30	6	4	0.016
	40	6	2	0.022
75	0	6	2	0.009
	10	6	2	0.014
	20	6	2	0.012
	30	6	2	0.017
	40	6	2	0.046
100	0	6	2	0.013
	10	6	2	0.015
	20	6	2	0.017
	30	6	5	0.022
	40	6	2	0.022

$$\text{RR} = \frac{1}{N^2} \sum_{i,j=1}^{N} R_{i,j} \qquad (4)$$

Its values range between 0 and 1, with 0 for no recurrences at all and 1 for complete recurrences, i.e., all times points are considered to belong to the same state. As mentioned above, RR depends on the threshold ε and, therefore, ε has to be selected with care. And also mentioned already, RR is chosen as 0.1 for all examined conditions in this study, in order to make the results comparable.

DET quantifies the ratio of recurrence points forming diagonals to all recurrent points. It is a measure of the predictability of the examined dynamical system and thus gives some indication about the nature of the dynamics (deterministic vs. random): high values of DET (approaching 1) indicates strong predictability of the dynamical system.

$$\text{DET} = \frac{\sum_{l=2}^{N} l P(l)}{\sum_{i,j}^{N} R_{i,j}}, \qquad (5)$$

where $P(l)$ is the histogram of the lengths l of diagonal lines in the RP.

ENTR is a measure of the complexity of the deterministic structure in the examined dynamic system, i.e. of the distribution of the diagonal lines $P(l)$. The measured ENTR refers to the Shannon entropy with respect to the probability $p(l)$ of finding a diagonal line of exactly length l in a RP, where

$$\text{ENTR} = - \sum_{l=l_{\min}}^{N} p(l) \ln p(l) \qquad (6)$$

where $p(l)$ is defined as follows,

$$p(l) = \frac{P(l)}{\sum_{l=l_{\min}}^{N} P(l)} \qquad (7)$$

ENTR is very low for uncorrelated noise, indicating the low complex nature of the dynamics, whereas for chaotic systems, ENTR is large.

LAM quantifies the percentage of recurrent points forming vertical lines in the RP; it indicates the extent of the laminar phases (intermittency) in the examined system.

$$\text{AM} = \frac{\sum_{\upsilon=2}^{N} \upsilon P(\upsilon)}{\sum_{\upsilon=1}^{N} \upsilon P(\upsilon)} \qquad (8)$$

$P(\upsilon)$ is the histogram of the lengths υ of vertical lines in the RP. LAM ranges between 0 and 1, with high values of LAM for laminar dynamics (exhibiting intermittency) and low values for absence of intermittent dynamics.

TT refers to the average length of the vertical lines, which can estimate the mean time that the system will abide at a specific state or how long a state will be trapped.

$$\text{TT} = \frac{\sum_{\upsilon=\upsilon_{\min}}^{N} \upsilon p(\upsilon)}{\sum_{\upsilon=\upsilon_{\min}}^{N} p(\upsilon)} \qquad (9)$$

3.4 Wavelet analysis

Wavelet analysis has certain benefits over the more traditional methods, such as Fourier transform and windowed Fourier transform. The classical Fourier transform simply performs frequency domain decomposition; it can be used to reveal the presence of periodicities, but it cannot localise those periodicities in time

[66]. By using a fixed-size window and then sliding the window in time, the windowed Fourier transform can apply the Fourier transform on a short segment of the signal [67], as such the temporal variations of the periodicities in a signal can be determined. However, a fixed-size window also means that the time resolution and the frequency resolution are fixed. Therefore, depending on the chosen window size, for a given signal, either the time localisation may be less precise or the frequency resolution may be poor. However, wavelet analysis provides an elegant way of adjusting the time and frequency resolutions in an adaptive fashion. Analogous to a zoom lens, a WT uses a window that narrows when focusing on small-scale or high-frequency features of the signal and widens on large-scale or low-frequency features [50,68] and it is particularly useful for analysing transient and intermittent phenomena. Therefore, recently wavelet analysis is well suited for the analysis of the fluctuations in internal combustion engines [41–43,46,49].

The continuous wavelet transform (CWT) of a discrete time series with respect to $\psi(t)$ is defined as [69]:

$$W_n(s) = \sum_{n'=1}^{N} \left(\frac{\delta t}{s}\right)^{1/2} x_{n'} \psi^* \left(\frac{(n'-n)\delta t}{s}\right), \qquad (10)$$

where $W_n(s)$ is the wavelet coefficient of the signal, the function $\psi(t)$ is a mother wavelet which is scaled and translated, the (*) represents the complex conjugate, δt is the sampling interval, $x_{n'}$ is the studied time series, parameters s and n are wavelet scale and localised time index, respectively. The amount of signal energy can be evaluated by the squared modulus of the CWT $|W_n(s)|^2$.

The analysing wavelet, $\psi(t)$, is a finite wave with zero mean and finite energy:

$$\int_{-\infty}^{+\infty} \psi(t)\, \mathrm{d}t = 0 \qquad (11)$$

In this study, a complex Morlet wavelet was used as the mother wavelet and is defined as:

$$\psi_0(\eta) = \pi^{-1/4} e^{i\omega_0 \eta} e^{-\eta^2/2}, \qquad (12)$$

where η is a non-dimensional "time," and ω_0 is the frequency. The value of ω_0 controls the number of oscillations in the mother wavelet and thus influences the frequency and time resolutions of the corresponding

wavelet transform [70–72]. In our study, we have chosen $\omega_0 = 6$ because this value can provide a good balance between time and frequency resolutions and satisfy the admissibility condition. The subscript 0 on ψ indicates that this $\psi(t)$ has been normalised [66].

4 Results

Figure 2 shows the IMEP time series for ethanol substitutions from 0 to 40% in 10% intervals at different load rates of 50%, 75% and 100%. At the top-right corner of each subgraph in Fig. 2a–c, there is an indicator—XXX-DYYYEZZZ, which represents the nominal XXX% of engine full load, the nominal YYY% of diesel fuel by energy and the nominal ZZZ% substitution of ethanol by energy. Figure 2 shows that the IMEP time series exhibits high-frequency small-scale fluctuations when the ethanol substitution is less than 20%, for all engine load rates. With an increase in ethanol substitution, long-periodic large-scale fluctuations occur and the fluctuation magnitude of the IMEP time series increases. However, when the same ethanol substitutions were used, the fluctuation frequency in the IMEP time series increases as the engine load rate increases.

Table 3 shows statistical properties. For an engine load rate of 50%, the standard deviation σ and the coefficient of inter-cycle variation based on IMEP (COV$_{\text{IEMP}}$) are lower when the ethanol substitution is 10%. At engine load rates of 75% and 100%, the combustion process is more stable using pure diesel. A clear observation is that the addition of ethanol leads to increased combustion variation. However, at an engine load rate of 75%, when compared to other ethanol substitutions, the COV$_{\text{IMEP}}$ is lowered with an ethanol substitution of 20%. For an engine load rate of 100%, the COV$_{\text{IMEP}}$ monotonically increases with respect to ethanol substitution.

Figure 3 depicts the return plots of the IMEP time series with ethanol substitutions from 0 to 40% at engine load rates of 50%, 75% and 100%. The resulting patterns reveal the evolution of the motion states in the combustion system attractor and the correlation between successive cycles. In order to more clearly reveal the structure characteristics of the combustion system attractors, the outlines of the attractors were artificially added. Note that a change in ethanol substitution has a significant effect on the geometric

Table 3 Statistical analysis result

Engine load rate (%)	Ethanol substitution (%)	IMEP	σ	COV$_{IMEP}$ (%)
50	0	0.874	0.010	1.19
	10	0.905	0.007	0.74
	20	0.890	0.008	0.89
	30	0.901	0.016	1.75
	40	0.886	0.030	3.36
75	0	1.263	0.007	0.52
	10	1.271	0.011	0.88
	20	1.267	0.010	0.78
	30	1.270	0.016	1.27
	40	1.251	0.051	4.07
100	0	1.647	0.010	0.58
	10	1.657	0.011	0.68
	20	1.645	0.013	0.76
	30	1.665	0.019	1.12
	40	1.666	0.019	1.16

structures of the combustion system attractors. For an ethanol substitution of 10% at an engine load rate of 50% and the pure diesel at an engine load rate of 75% cases, the patterns of the phase space reconstruction possess relatively regular circular structures with a smaller diameter attractor, which corresponds to smaller combustion fluctuation. However, for the other ethanol substitutions and pure diesel cases at all engine load rates, the attractors possess an elliptical structure. Furthermore, the patterns in return maps appear to show increased asymmetry about the diagonal, and hence, time irreversibility as the ethanol substitution increases. At a specific engine load rate, with an increase in the ethanol substitution, the scales of the elliptical combustion system attractors on the main diagonal direction (long axis direction) are elongated. However, at the same ethanol substitution, with an increase of engine load rate, the short axis radii of the attractors increase.

Figure 4 shows the RPs when the ethanol substitution ranges from 0 to 40% at engine load rates of 50%, 75% and 100%. In Fig. 4, the data, including all of the testing cycles, were used to reveal the long-term dynamic behaviour of the combustion system when different ethanol substitutions were used. In order to more clearly exhibit the internal texture of Fig. 4, a small-scale pattern, which includes partial cycles, was embedded in the top-right corner of each subgraph. From Fig. 4, it is clear that the patterns in the RPs change

significantly as the ethanol substitution increases; the textures in the RPs and the influence of the ethanol substitution on the dynamics of the combustion system in a dual-fuel engine are very different at different engine loads.

For engine load rates of 50%, when the ethanol substitution is 0% (pure diesel) and 10%, the RPs depict rather homogeneous and denser recurrence structures, which consist of a lot of small blocks, short diagonals and horizontal or vertical lines. For pure diesel mode, long diagonals parallel to the main diagonal can be clearly observed in the small-scale pattern. For the 10% ethanol substitution case, the vertical lines indicate the presence of laminar states or intermittency in the IMEP time series, and at the same time, the RP in the small-scale patterns exhibits many clear dashed diagonal lines with different lengths and distance. When the ethanol substitution is 20%, the RP consists mainly of dashed diagonal lines and white bands. In all of the above three cases, the longer diagonal line structure corresponds to more stable combustion and small-scale fluctuations and short diagonals express the high variability and the fast change of the system states. With a further increase in ethanol substitution, an obvious grid (consisting of the white areas and black blocks) occurs, and the scale of the white areas and black blocks in the grid increases. Such white areas correspond to abrupt changes in the dynamics and mark epochs of more frequently occur-
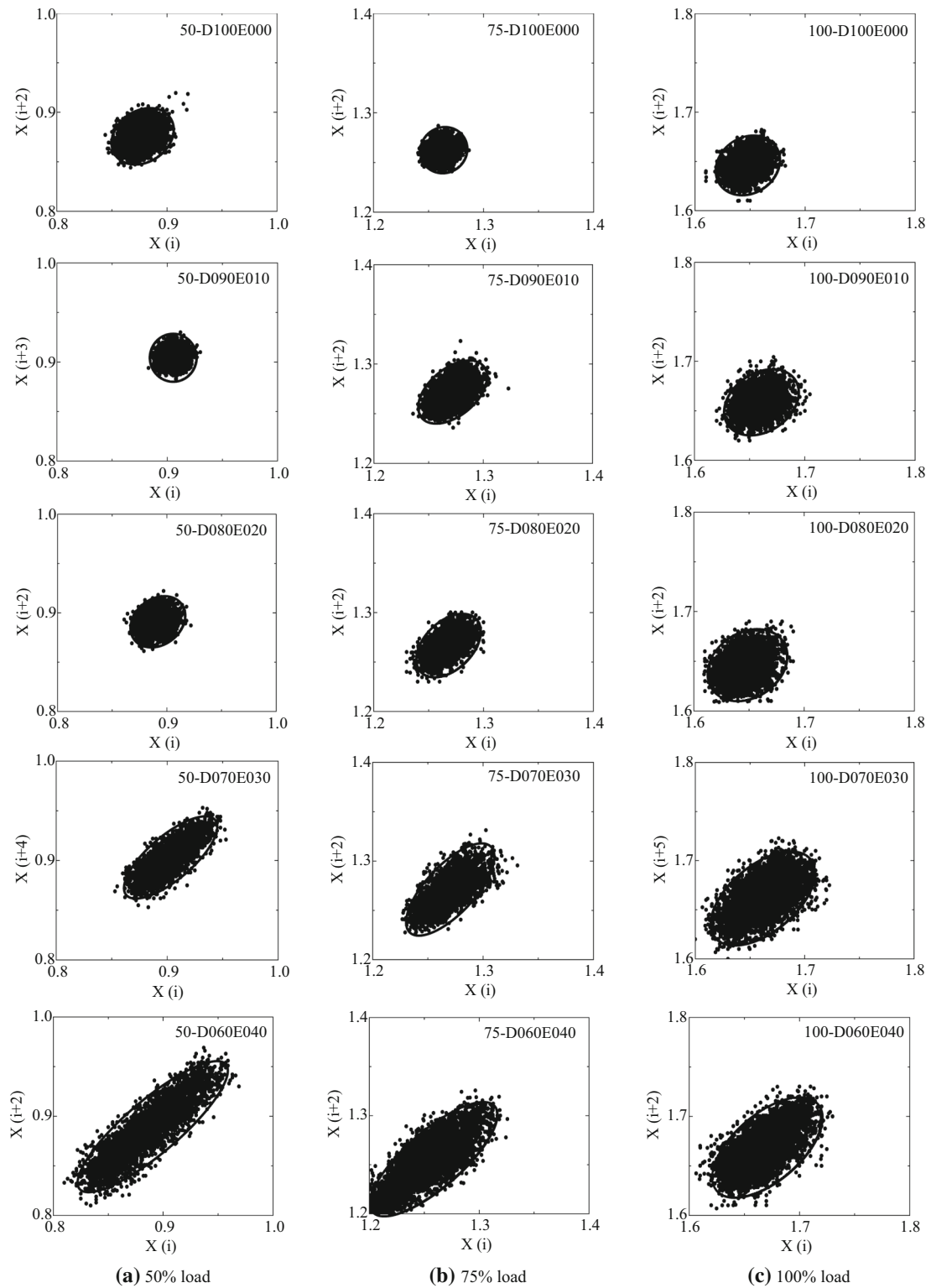
Fig. 3 Return plots of IMEP time series when ethanol substitution is from 0 to 40% under different load rates of 50%, 75% and 100%
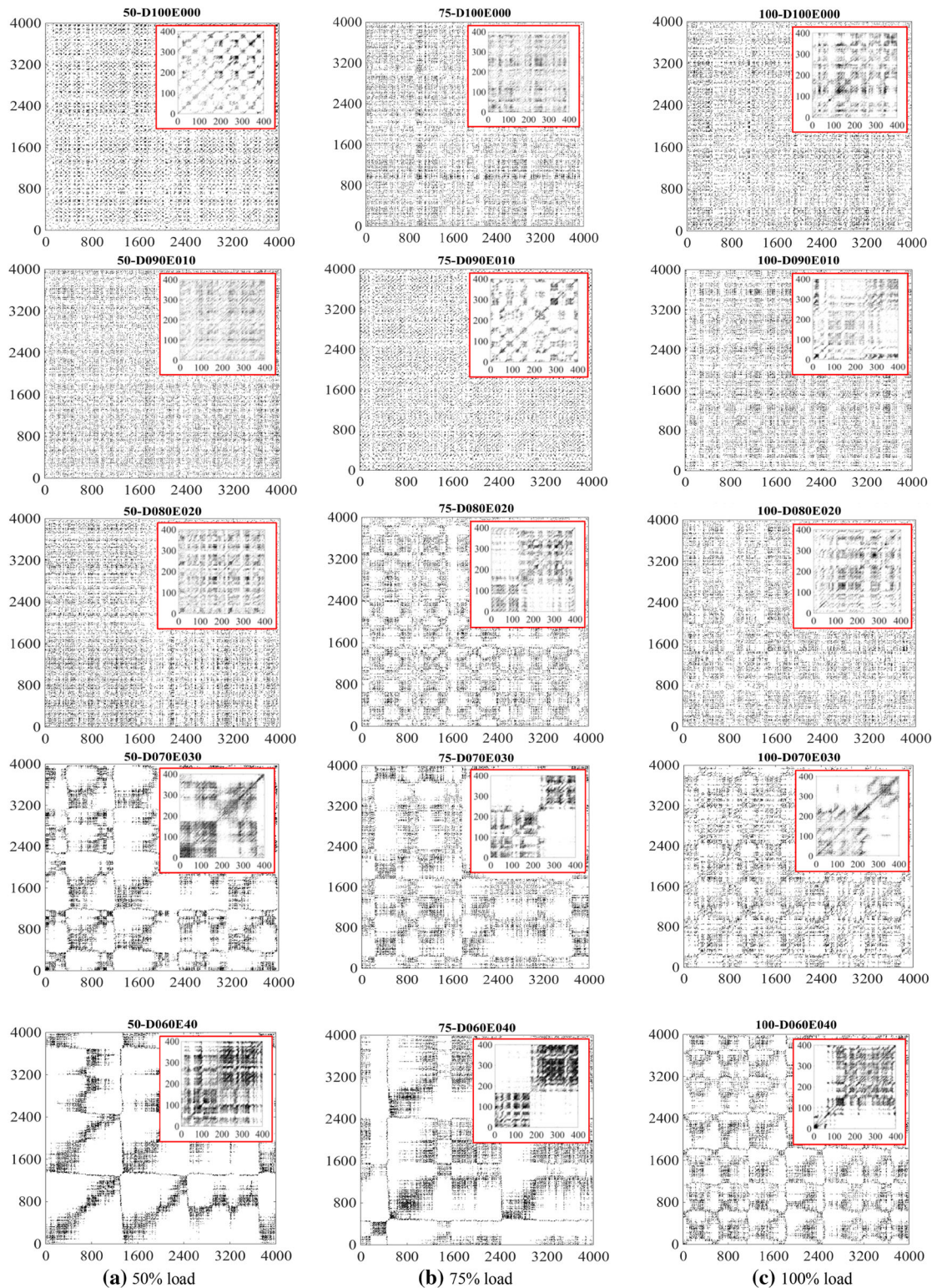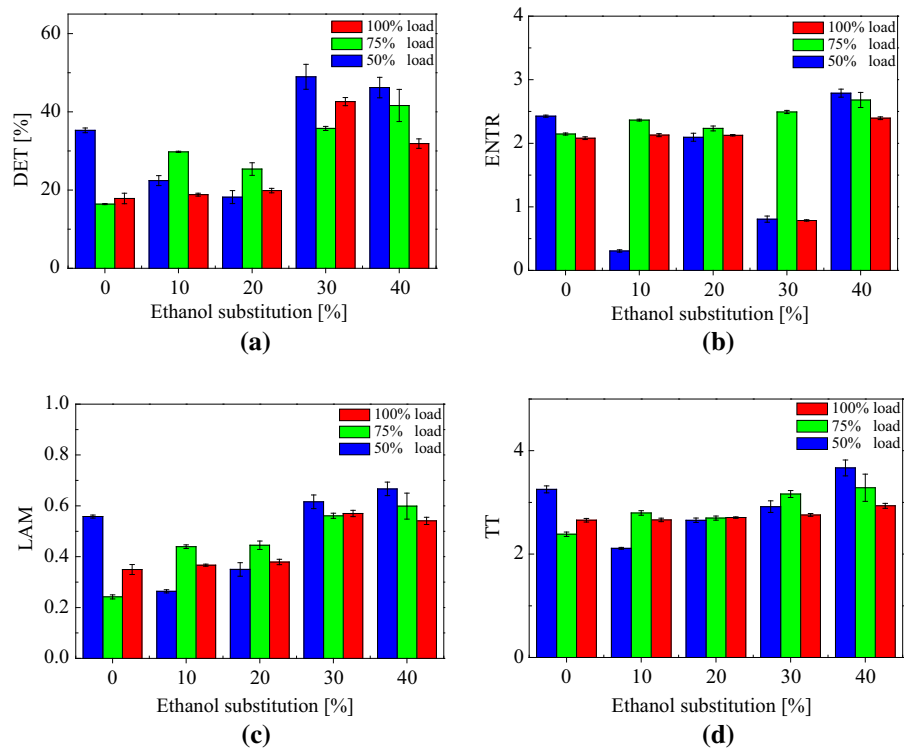
Fig. 4 RPs when the ethanol substitution ranges from 0 to 40% under different load rates of 50%, 75% and 100%

Fig. 5 RQA measures when ethanol substitution is from 0 to 40% under different load rates of 50%, 75% and 100%

ring extreme combustion events. However, in small-scale RPs, a number of diagonal lines and blocks can be readily seen.

For engine load rate of 75%, the RP in pure diesel mode is similar to the RP using an ethanol substitution of 10% at an engine load rate of 50%. The RP for pure diesel consists of many dashed diagonal lines, while the RP using an ethanol substitution of 10% at an engine load rate of 75% is similar to the RP of pure diesel at an engine load rate of 50%, where the RP possesses a long diagonal structure. With an increase in ethanol substitution, the grid structure occurs and the scale of square blocks in the grids increase gradually. Compared to an engine load rate of 50%, the grid structure in the RPs occurs earlier (with an ethanol substitution of 20%) and the scale of the grid is larger at load rates of 75%. In small-scale patterns, the internal textures of the RPs are gradually divided into four separate areas: two white areas and two grid areas. Interestingly, with the change of ethanol substitution, the scale and texture of the RPs constantly transform from one distribution to another.

When the engine operates at an engine load rate of 100%, ethanol fumigation also has a significant effect

on the structure of the RPs. However, compared to engine load rates of 50% and 75%, the structures of the RPs in large-scale patterns are more regular and richer at each ethanol substitution. The RP for pure diesel conditions consists of diagonal lines and clusters of black blocks; the fluctuations in the combustion process reveal high-frequency quasi-periodic behaviours. With an increase in ethanol substitution, the scale of diagonal lines and black blocks increases, the patterns become more distinct. Especially, at ethanol substitutions of 30% and 40%, the RPs possess more regular grid structures with a homogeneous distribution, and the scale of the grids is smaller for an engine load rate of 100%, and this means the more regular combustion fluctuations appear.

Overall, for all engine loads, when higher ethanol substitution is adopted, the combustion system will exhibit long-period large-scale regular fluctuation behaviours.

RQA measures (DET, ENTR, LAM and TT) were calculated to further quantitatively analyse the dynamic characteristics of the combustion system. Figure 5 depicts the results of the RQA measures. DET and ENTR are two RQA measures based on diagonal lines.

From Fig. 5a, note that for an engine load rate of 50%, as the ethanol substitution increases from 0 to 20%, the DET decreases from 35.3 ± 0.6 to $18.2 \pm 1.7\%$ and then increases to $48.9 \pm 3.2\%$ when the ethanol substitution is 30%, but there is only a small difference between the values of DET for ethanol substitutions of 30% and 40%. When the engine operates at an engine load rate of 75%, the values of DET present an increasing trend as the ethanol substitution increases, except for an ethanol substitution of 20%. For an engine load rate of 100%, when the ethanol substitution is less than 30%, the DET monotonically increases with an increase in ethanol substitution, while the DET decreases when the ethanol substitution is higher than 30%.

Considering the ENTR, we find that the complexity of the combustion system is sensitive to the addition of ethanol, especially under lower engine load conditions with higher ethanol substitution (Fig. 5b). For an engine load rate of 50%, when the ethanol substitution ranges from 0 to 40%, there are two minimum values of ENTR. This means that when the ethanol substitution is 10% and 30%, the complexities of the combustion system were reduced, but higher ethanol substitutions lead to more complex combustion fluctuations. For an engine load rate of 75%, with increasing ethanol substitutions, values of ENTR progressively increased, but the difference between the values of ENTR is small. This means that the engine has a high tolerance to the ethanol substitution. At full engine load (100%), a small amount of ethanol addition has almost no effect on the complexity of the combustion system. When the ethanol substitution is less than 20%, the values of ENTR are held nearly constant (2.1 ± 0.02). An ethanol substitution of 30% is beneficial to reduce the complexity of the combustion fluctuations. However, excessive use of ethanol leads to deterioration in engine performance.

LAM and TT are two RQA measures based on the vertical structures. Figure 5c presents that for an engine load rate of 50%, with increasing ethanol substitutions, values of LAM initially decrease before later increasing at the higher ethanol substitutions. The minimum value of LAM (0.264 ± 0.006) occurs at an ethanol substitution of 10%. This clearly indicates a transition of combustion process from a more laminar to a less laminar state as the ethanol substitution increases from 0 to 10% and a transition from a less laminar to a more laminar state when the ethanol substitution increases from 10 to 40%. For an engine load of 75%, the values of LAM increase from 0.242 ± 0.008 to 0.599 ± 0.005 when

the ethanol substitution ranges from 0 to 40%. When the engine operates at an engine load rate of 100%, except for an ethanol substitution of 40%, the values of LAM gradually increase with increasing ethanol substitutions. Note that from Fig. 5d, the minimum value of TT (2.111 ± 0.018) occurs at an ethanol substitution of 10% for an engine load rate of 50%; however, for engine load rates of 75% and 100%, the values of TT monotonically increase with increasing ethanol substitutions.

Figures 6, 7 and 8 show the wavelet power spectrums (WPS) when the ethanol substitution ranges from 0 to 40% at engine load rates of 50%, 75% and 100%. In these figures, the horizontal axis denotes the number of cycles, the vertical axis represents the period in cycles, and the different colour indicates the associated power level. Blue and red donate the lowest and highest power levels, respectively. Intermediate power levels are represented by the other colours. Note that there is a dark U-shaped curve in each subgraph of Figs. 6, 7 and 8 and the region below the U-shaped curve is called the cone of influence (COI). Inside the COI, the edge effects become important, and the results in this region may be unreliable and should be interpreted with caution [67, 70].

For the engine load rate of 50%, the WPSs reveal the presence of multiple periodicities when the ethanol substitution is less than 30%. For example, it is very clear for the pure diesel mode that there is a high spectral power in a band around the 80-cycle period which persists for the entire 4000 engine cycles. The high-frequency intermittent fluctuations in the 40-cycle band can be readily seen in this figure; however, they appear in an intermittent fashion and persist over a brief interval. There are also a few weaker cycle bands which appear between 128-cycle period and 256-cycle period as well as near the cone of influence (COI). Interestingly, when 10% fumigation ethanol is substituted, the ICV exhibits intermittent fluctuation characteristics around the three main cycle periods: 48-cycle period, 96-cycle period and 256-cycle period. As the ethanol substitution is increased from 20 to 40%, the intermittent short-term fluctuations fade away, the combustion process exhibits long-term fluctuations, and the most prominent periodicity appears near the COI.

For the engine load rate of 75%, except for the ethanol substitution of 10%, all the periodic bands with the strongest power intensity appear in the low-frequency region bordering the COI and nearly per-
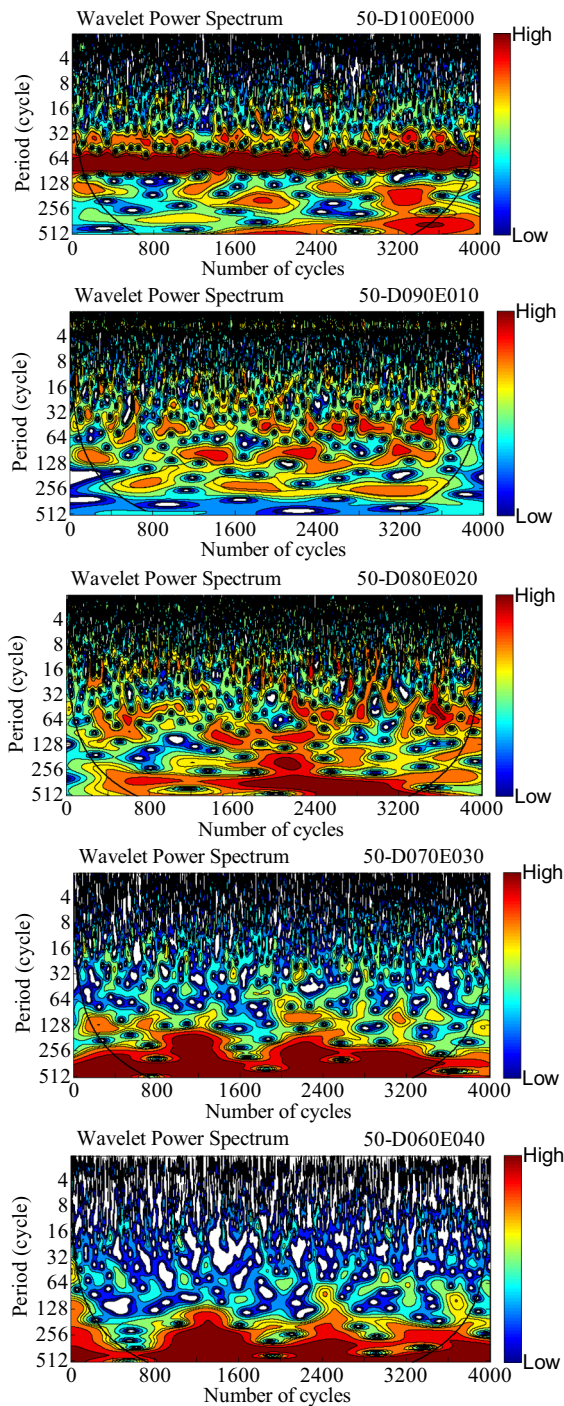
Fig. 6 Wavelet power spectrum (WPS) when ethanol substitution is from 0 to 40% under load rate of 50%
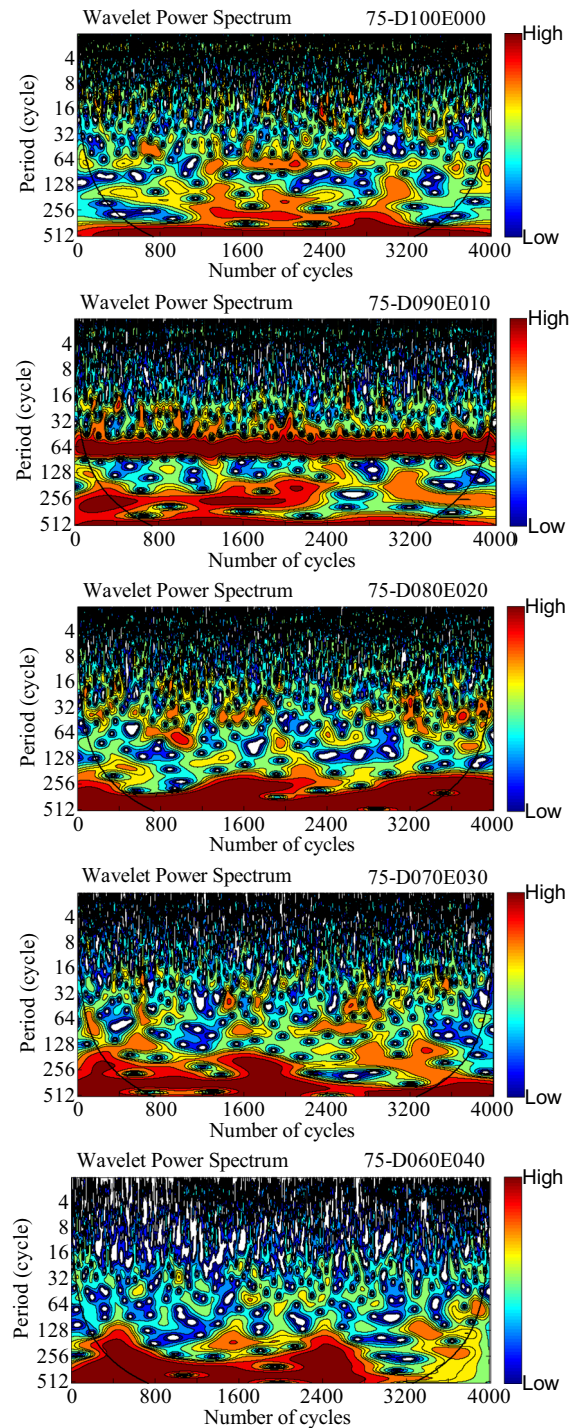
Fig. 7 Wavelet power spectrum (WPS) when ethanol substitution is from 0 to 40% under load rate of 75%
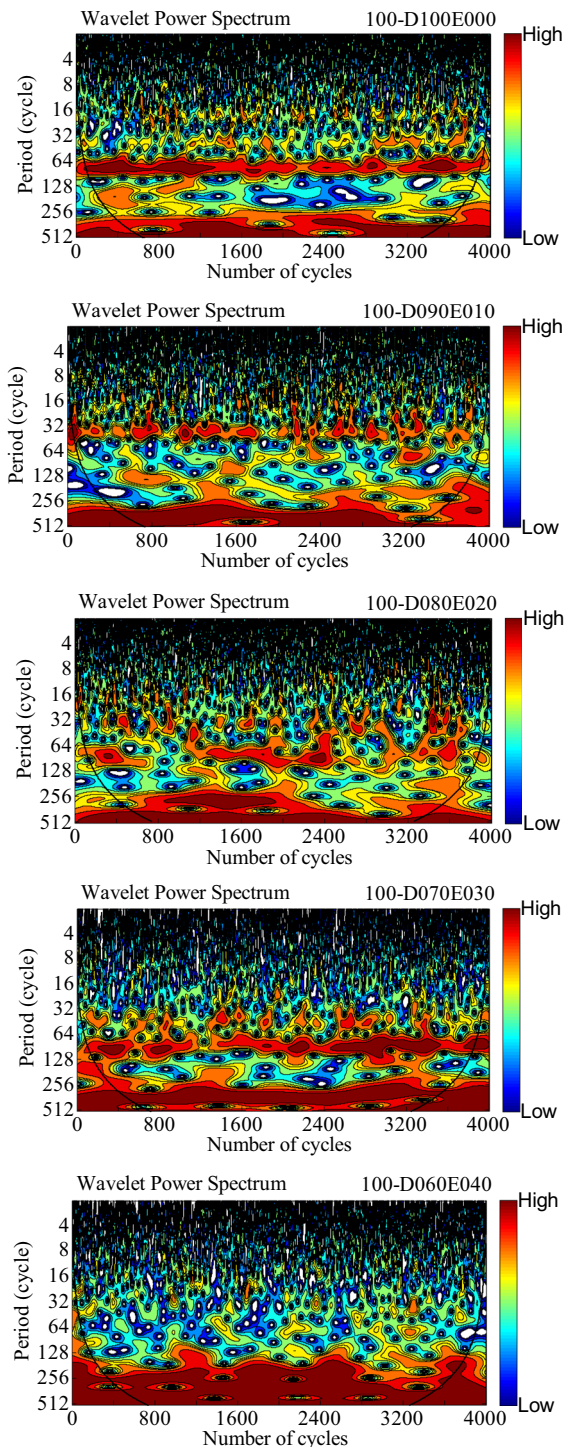
Fig. 8 Wavelet power spectrum (WPS) when ethanol substitution is from 0 to 40% under load rate of 50%

sist for the entire 4000 engine cycles, and there are only a few weaker sporadic variations. WPS for the ethanol substitution of 10% also reveals multiple periodicities. The most prominent periodicities in the figure appear around the three-cycle bands; they are as follows: (a) the high spectral power in a band appears around the 64-cycle period and it lasts over the entire engine cycles, (b) a similar high-power periodic band bordering the COI is also observed, which lasts over engine cycles 650–3300, and (c) the periodic bands around 256-cycle period—they persist from approximately 400–600 cycles and 1200–2000 cycles, respectively.

For the engine load of 100%, the WPS is also sensitive to the addition of ethanol, and multiple periodicities are very obvious. Among these bands, the two most prominent periodic bands are readily identified and persist for nearly the entire 4000 engine cycles; one of the prominent periodic bands constantly appear near the COI, and the another prominent periodic band changes between the 32-cycle period and the 256-cycle period. The main variation trend of the changeable periodic band is that it moves towards the low-frequency fluctuation region as the ethanol substitution increases. In addition, we can observe a few weaker periodicities for each ethanol substitution and several short-term periodicities in intermittent.

Evident is that the addition of ethanol has a significant effect on combustion fluctuations and dynamic complexities in a modern ethanol–diesel dual-fuel engine. Based on the RPs, RQA and wavelet analysis at different engine load rates, insight into the dynamic behaviours of the combustion system when different ethanol substitutions were used could be gained. For all studied engine loads, at pure diesel mode and lower ethanol substitutions, we can observe the presence of multiple periodicities combined with the high-frequency intermittent fluctuations, and as the ethanol substitution increases, persistent low-frequency fluctuations gradually play a predominant role in the multi-cycle combustion process. In comparison, at a lower engine load, the dynamics of the combustion system is more sensitive to the addition of ethanol, e.g. a proper ethanol substitution can lead to more stable combustion corresponding to the regular and smaller combustion system attractors and reduced complexities. However, high ethanol substitutions lead to large-scale low-frequency combustion fluctuations and increased complexities. For higher engine loads, higher ethanol sub-

stitution is acceptable because the heat absorbed by the evaporation of ethanol does not play predominant role in the process of ignition and combustion. However, excessive addition of ethanol also leads to increased complexities and more laminar states, which correspond to the abrupt changes in the combustion process and more frequently occurring extreme or rare combustion events. This may be caused by auto-ignition of the ethanol and air mixture prior to diesel injection in some engine combustion cycles.

5 Discussion

By investigating the start of combustion timing, insight into the generating mechanism of the above combustion phenomenon and possible explanations for the dynamic behaviour can be sought out. In this study, ethanol was injected into the inlet manifold between the turbocharger and inter-cooler during the intake stroke. As there is a long distance from the position of the ethanol injector to the intake valves, it can be assumed that a homogeneous mixture goes into the combustion chamber.

If in-cylinder pressure and temperature reach certain values, auto-ignition combustion will occur before diesel injection. Such combustion is termed homogeneous charge compression ignition (HCCI) [73,74]. Diffusion combustion of diesel starts after the diesel fuel is injected into the high-temperature mixture of air and ethanol. However, if the in-cylinder environment does not reach a sufficient temperature and pressure to cause the auto-ignition of the homogenous mixture of air and ethanol, the mixture will be ignited by the diesel.

Comparing to a mechanical diesel injection system in a traditional diesel engine, the high-pressure common-rail diesel injection system in a modern diesel engine can produce better diesel atomisation. As a consequence, there are more diesel oil droplets which can be used as the ignition source of the air and ethanol mixture. The combustion speed in cylinder is controlled by the speed of evaporation, diffusion and combustion of diesel droplets, so such a combustion mode is mixing-controlled combustion [75]. Furthermore, at some conditions, with high temperature and high pressure, compound combustion including HCCI combustion and mixing-controlled combustion may occur in an ethanol-fumigated dual-fuel engine. It is obvious that the combustion process in a dual-fuel engine is more complex than a pure diesel engine. The different combustion modes influence each other by flame propagation or transmission of heat and mass. It is important to further reveal the transition of the combustion mode and its influence on combustion fluctuations and the nonlinear dynamics of the combustion system. Therefore, the diesel injection timing was acquired by directly interrogating the electronic diesel injector driver signal, and the start of pre-mixed or diffusion combustion was determined by isolating the resonant frequency information using the Bayesian approach [22]. Ignition delay was calculated by comparing the injection timing of the diesel and the start of combustion.

Figure 9 depicts the probability density functions (PDF) of the start of diesel injection, the start of combustion and ignition delay for different ethanol substitutions at engine load rates of 50%, 75% and 100%. It is clear from Fig. 6 that the diesel injection timing was systematically retarded with increasing ethanol substitutions. However, the biggest difference between injection timing signals of diesel is no more than 1.5 crank angle degrees (°CA) for different ethanol substitutions at an engine load rate of 75%.

When the engine operated at a load rate of 50%, except for the 10% ethanol substitution case, the start of combustion was retarded, and the ignition delay and probability distribution range increased with an increase in ethanol substitution. For all ethanol substitutions, the probability distribution range of the ignition delay is wider than that of pure diesel. At an ethanol substitution of 10%, the start of combustion in some cycles was advanced before diesel combustion because ethanol is an oxygenated fuel which can facilitate the oxidation and combustion of diesel. The more important reason is that at this time the "cooling effect" is not predominant due to the lower mass flow rate of ethanol. Therefore, the combustion is more stable, and the smaller values of ENTR and LAM imply the reduced complexities and less laminar states of the combustion system. At 50% engine load, for all ethanol substitutions, no auto-ignition occurs—the start of combustion occurs after diesel injection. The mixture of air and ethanol needs be ignited by diesel; therefore, the start of combustion depends on the injection timing of the diesel. In these cases, combustion should be mixing-controlled combustion. Such combustion is caused by the lower in-cylinder combustion pressure and temperature. In addition, compared

Fig. 9 Start of diesel injection, start of combustion and ignition delay for different ethanol substitution at engine loads of 50%, 75% and 100%

(a) start of diesel injection and start of combustion

(b) ignition delay
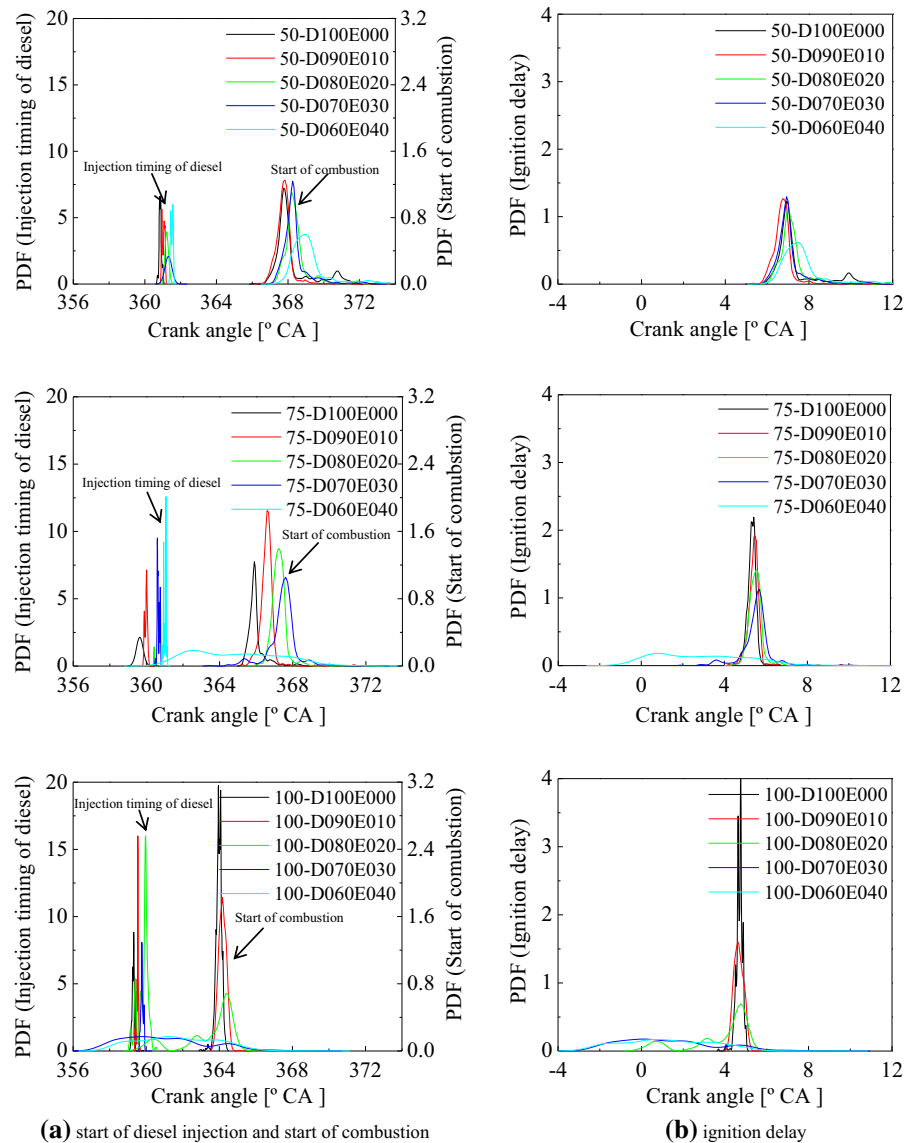
to higher engine load rates (75% and 100%), at the same ethanol substitution, the in-cylinder mixture is leaner, so it is less likely to have auto-ignition. In particular, it is given that the auto-ignition temperature of ethanol is 423 °C, which is significantly higher than diesel (270 °C).

When the engine operates at an engine load rate of 75%, compared to pure diesel operation, the start of combustion is retarded and the ignition delay systematically increases as the ethanol substitution increases from 0 to 30%. The unimodal distribution characteristics of ignition delay can be observed for the ethanol

substitutions of 0%, 10% and 20%, and the probability distribution range of ignition delay is relatively small. This means that the combustion process is not sensitive to the addition of ethanol when the ethanol substitution is less than 30%, so there is no obvious change in the complexities of the combustion system (see Fig. 5b). At this time, the mixture of air and ethanol is leaner, the auto-ignition condition cannot be met, and the ignition and combustion of the mixture of air and ethanol predominantly depend on the injection timing of the diesel. Therefore, the combustion is mixing controlled. For the ethanol substitution of 30%, it is predominantly show-

ing later combustion than the neat diesel case. However, there are some cycles where the start of combustion is earlier, and the distribution of the start of combustion is quite multimodal. This phenomenon indicates that the compound combustion mode occurs occasionally because the start of combustion in some cycles is earlier than that of pure diesel operation. With a further increase in ethanol substitution, the probability density distribution ranges of the ignition delay increase. Interestingly, some combustion cycles with negative ignition delay can be seen for the ethanol substitution of 40%. This further demonstrates the increased proportion of HCCI combustion in the whole energy-release process.

For an engine load rate of 100%, it is evident that ethanol substitution leads to an advanced start of combustion and an increase in the probability density distribution ranges of ignition delay for all ethanol substitutions. At an ethanol substitution of 10%, predominant combustion mainly occurs slightly later than that of pure diesel. The most predominant combustion at the ethanol substitution of 20% occurs later than both the pure diesel and the ethanol substitution of 10% cases. For all ethanol substitutions, the start of combustion in some cycles is earlier than pure diesel, and the probability of such a cycle occurrence increases with increasing ethanol substitution. This means that once ethanol is introduced into the dual-fuel engine at an engine load rate of 100%, higher in-cylinder pressure and temperature leads to the auto-ignition of the air and ethanol mixture. Moreover, compared to engine load rates of 50% and 75%, at the same ethanol substitution, the mass flow rate of ethanol is higher, and the mixture of air and ethanol is richer, so this is another condition promoting the occurrence of auto-ignition combustion of ethanol and air mixture. It is evident that the proportion of energy release of HCCI combustion in whole compound combustion in-cylinder increases with increasing ethanol substitutions. At an ethanol substitution of 30%, the value of ENTR is significantly lower than other ethanol substitutions, which is equal to 0.79 ± 0.01. However, the value of ENTR at an ethanol substitution of 40% rapidly increases to 2.40 ± 0.02. So, for high engine loads, at the higher ethanol substitutions, the large-scale low-frequency combustion fluctuations and increased complexities are caused by cyclic excitation oscillation during the transition of the combustion mode.

6 Conclusion

In this study, the fluctuation features and dynamic complexities of the indicated mean effective pressure (IMEP) time series from an ethanol-fumigated dual-fuel engine have been qualitatively and quantitatively analysed. This analysis was based on nonlinear embedding theory and by calculating recurrence plots (RPs), measures of recurrence quantification analysis (RQA) and wavelet analysis. The transition characteristics of the combustion mode and the correlation with dynamic behaviours of the combustion system have been revealed. The conclusions we have carried out are as follows:

(1) For all engine load rates, ethanol fumigation has a significant effect on the combustion fluctuations. For pure diesel mode and lower ethanol substitutions, the ICV at different engine loads exhibits multiscale dynamics consisting of strongly periodic and/or intermittent fluctuations. With an increase in the ethanol substitution, large-scale low-frequency fluctuations become more predominant. However, compared to high engine loads (75% and 100%), the combustion fluctuations and the dynamics of the combustion system at an engine load of 50% are more sensitive to ethanol substitution.

(2) Except for the ethanol substitution of 10% at an engine load rate of 50% and pure diesel at an engine load rate of 75%, the attractors of the combustion system possess elliptical structures. With an increase in ethanol substitution, the scales of the elliptical combustion system attractors on the main diagonal direction are elongated. At the same ethanol substitutions, with an increase in engine load rate, the short axis radii of the attractors increase.

(3) For all engine loads, the patterns in the RPs change significantly as the ethanol substitution increases. When the ethanol substitution is less than 20%, the RPs depict rather homogeneous and denser recurrence structures corresponding to the more stable combustion, and the vertical lines in RPs indicate the presence of intermittency in the IMEP time series, which is consistent with the results of wavelet analysis. When the ethanol substitution is higher than 20%, an obvious grid structure occurs. Such white areas correspond to abrupt changes in

the dynamics and mark epochs of more frequently occurring auto-ignition combustion.

(4) At an engine load rate of 50%, for all of the ethanol substitutions, the start of combustion always occurs after diesel injection, indicating there is only mixing-controlled combustion, and the enhanced cooling caused by excessive ethanol evaporation plays a predominant role—which causes increased ignition delay and abrupt changes in the dynamics as well as increased complexities of the combustion system. However, for higher engine load rates, there are obvious combustion mode transitions from mixing-controlled combustion to compound combustion, which causes the long-periodic large-scale fluctuations and increased complexities in the combustion system.

Compliance with ethical standards

Conflict of interest The authors declare that they have no conflict of interest.

References

1. Tutak, W.: Bioethanol E85 as a fuel for dual-fuel diesel engine. Energy Convers. Manag. **86**, 39–48 (2014). https://doi.org/10.1016/j.enconman.2014.05.016

2. Wheals, A.E., Basso, L.C., Alves, D.M.G., Amorim, H.V.: Fuel ethanol after 25 years. Tibtech **17**, 482–7 (1999). https://doi.org/10.1016/S0167-7799(99)01384-0

3. Imran, A., Varman, M., Masjuki, H.H., Kalam, M.A.: Review on alcohol fumigation on diesel engine: available alternative dual-fuel technology for satisfactory engine performance and reduction of environment concerning emission. Renew Sustain. Energy Rev. **26**, 739–751 (2013). https://doi.org/10.1016/j.rser.2013.05.070

4. Kumar, K., Sung, C.J.: A comparative experimental study of the autoignition characteristics of alternative and conventional jet fuel/oxidizer mixtures. Fuel **89**, 2853–63 (2010). https://doi.org/10.1016/j.fuel.2010.05.021

5. Fraioli, V., Mancaruso, E., Migliaccio, M., Vaglieco, B.M.: Ethanol effect as premixed fuel in dual-fuel CI engines: experimental and numerical investigations. Appl. Energy **119**, 394–404 (2014). https://doi.org/10.1016/j.apenergy.2014.01.008

6. Tsang, K.S., Zhang, Z.H., Cheung, C.S., Chan, T.L.: Reducing emissions of a diesel engine using fumigation ethanol and a diesel oxidation catalyst. Energy Fuels **24**, 6156–65 (2010). https://doi.org/10.1021/ef100899z

7. Rodríguez-Fernández, J., Tsolakis, A., Theinnoi, K., Snowball, J., Sawtell, A., York, A.P.E.: Engine performance and emissions from dual-fuelled engine with in-cylinder injected diesel fuels and in-port injected bioethanol. SAE paper, no. 2009-01-1853 (2009). https://doi.org/10.4271/2009-01-1853

8. Pedrozo, V.B., May, I., Nora, M.D., Cairns, A., Zhao, H.: Experimental analysis of ethanol dual-fuel combustion in a heavy-duty diesel engine: an optimisation at low load. Appl. Energy **165**, 6–182 (2016). https://doi.org/10.1016/j.apenergy.2015.12.052

9. Mancaruso, E., Vaglieco, B.M.: Spectroscopic analysis of the phases of premixed combustion in a compression ignition engine fuelled with diesel and ethanol. Appl. Energy **143**, 164–175 (2015). https://doi.org/10.1016/j.apenergy.2015.01.031

10. Ekholm, K., Karlsson, M., Tunestål, P., Johansson, R., Johansson, B., Strandh, P.: Ethanol-diesel fumigation in a multi-cylinder engine. SAE paper, no. 2008-01-0033 (2008). https://doi.org/10.4271/2008-01-0033

11. Padala, S., Woo, C.H., Kook, S.H., Hawkes, E.R.: Ethanol utilisation in a diesel engine using dual-fuelling technology. Fuel **109**, 597–607 (2013). https://doi.org/10.1016/j.fuel.2013.03.049

12. Abu-Qudais, M., Haddad, O., Qudaisat, M.: The effect of alcohol fumigation on diesel engine performance and emissions. Energy Convers. Manag. **41**, 389–399 (2000). https://doi.org/10.1016/S0196-8904(99)00099-0

13. Chen, J., Gussert, D., Gao, X., Gupta, C., Foster, D.: Ethanol fumigation of a turbocharged diesel engine. SAE paper, no. 810680 (1981). https://doi.org/10.4271/810680

14. Hayes, T.K., Savage, L.D., White, R.A., Sorenson, S.C.: The effect of fumigation of different ethanol proofs on a turbocharged diesel engine. SAE paper no. 880497 (1988). https://doi.org/10.4271/880497

15. Ajav, E.A.S., Bachchan, B.T.K.: Thermal balance of a single cylinder diesel engine operating on alternative fuels. Energy Convers. Manag. **41**, 1533–1541 (2000). https://doi.org/10.1016/S0196-8904(99)00175-2

16. Udayakumar, R., Sundaram, S., Sivakumar, K.: Engine performance and exhaust characteristics of dual-fuel operation in DI diesel engine with methanol. SAE paper no. 2004-01-0096 (2004). https://doi.org/10.4271/2004-01-0096

17. Asad, U., Kumar, R., Zheng, M., Tjong, J.: Ethanol-fueled low temperature combustion: a pathway to clean and efficient diesel engine cycles. Appl. Energy **157**, 838–850 (2015). https://doi.org/10.1016/j.apenergy.2015.01.057

18. Zhang, Z.H., Tsang, K.S., Cheung, C.S., Chan, T.L., Yao, C.D.: Effect of fumigation methanol and ethanol on the gaseous and particulate emissions of a direct-injection diesel engine. Atmos. Environ. **45**, 2001–2008 (2011). https://doi.org/10.1016/j.atmosenv.2010.12.019

19. Popa, M., Negurescu, N., Pana, C., Racovitza, A.: Results obtained by methanol fuelling diesel engine. SAE paper no. 2001-01-3748 (2001). https://doi.org/10.4271/2001-01-3748

20. Heisey, J.B., Lestz, S.S.: Aqueous alcohol fumigation of a single-cylinder DI diesel engine. SAE paper no. 811208 (1981). https://doi.org/10.4271/811208

21. Di Blasio, G., Beatrice, C., Molina, S.: Effect of port injected ethanol on combustion characteristics in a dual-fuel light

duty diesel engine. SAE paper no. 2013-01-1692 (2013). https://doi.org/10.4271/2013-01-1692

22. Bodisco, T., Low Choy, S., Brown, R.J.: A Bayesian approach to the determination of ignition delay. Appl. Therm. Eng. **60**, 79–87 (2013). https://doi.org/10.1016/j.applthermaleng.2013.06.048

23. Bodisco, T., Tröndle, P., Brown, R.J.: Inter-cycle variability of ignition delay in an ethanol fumigated common-rail diesel engine. Energy **84**, 186–195 (2015). https://doi.org/10.1016/j.energy.2015.02.107

24. Bodisco, T., Brown, R.J.: Inter-cycle variability of in-cylinder pressure parameters in an ethanol fumigated common-rail diesel engine. Energy **52**, 55–65 (2013). https://doi.org/10.1016/j.energy.2012.12.032

25. Barton, R.K., Kenemuth, D.K., Lestz, S.S., Meyer, W.E.: Cycle-by-cycle variations of a spark ignition engine: a statistical analysis. SAE paper no. 700488 (1970). https://doi.org/10.4271/700488

26. Ozdor, N., Dulger, M., Sher, E.: Cyclic variability in spark-ignition engines: a literature survey. SAE paper no. 940987 (1994). https://doi.org/10.4271/940987

27. Finney, C.E.A., Kaul, B.C., Daw, C.S., Wagner, R.M., Edwards, K.D., Green, J.B.: A review of deterministic effects in cyclic variability of internal combustion engines. In. J. Engine Res. **16**(3), 366–378 (2015). https://doi.org/10.1177/1468087415572033

28. Barton, R.K., Kenemuth, D.K., Lestz, S.S., Meyer, W.E.: Cycle-by-cycle variations of a spark ignition engine: a statistical analysis. SAE paper no. 700488 (1970)

29. Belmont, M.R., Hancock, M., Buckingham, D.J.: Statistical aspects of cyclic variability. SAE paper no. 860324 (1986)

30. Martin, J.K., Plee, S.L., Remboski Jr., D.J.: Burn modes and prior-cycle effects on cyclic variations in lean burn spark-ignition engine combustion. SAE paper no. 880201 (1988). https://doi.org/10.4271/880201

31. Moriyoshi, Y., Kanimoto, T., Yagita, M.: Prediction of cycle-to-cycle variation of in-cylinder flow in a motored engine. SAE paper no. 930066 (1993). https://doi.org/10.4271/930066

32. Daw, C.S., Finney, C.E.A., Green, J.B., et al.: A simple model for cyclic variations in a spark-ignition engine. SAE paper, no. 962086 (1996). https://doi.org/10.4271/962086

33. Daily, J.W.: Cycle-to-cycle variations: a chaotic process? Combust. Sci. Technol. **57**, 149–62 (1988). https://doi.org/10.1080/00102208808923950

34. Gotoda, H., Okuno, Y., Hayashi, K., Tachibana, S.: Characterization of degeneration process in combustion instability based on dynamical systems theory. Phys. Rev. E **92**, 052906 (2015). https://doi.org/10.1103/PhysRevE.92.052906

35. Godavarthi, V., Pawar, S.A., Unni, V.R., Sujith, R.I., Marwan, N., Kurths, J.: Coupled interaction between unsteady flame dynamics and acoustic field in a turbulent combustor. Chaos **28**, 113111 (2018)

36. Bassily, H., Daqaq, M.F., Wagner, J.: Application of the pseudo-poincare maps to assess gas turbine system health. ASME J. Gas Turbines Power **134**, 051601-1–8 (2012)

37. Wendeker, M., Litak, G., Czarnigowski, J., Szabelski, K.: Nonperiodic oscillations in a spark ignition engine. Int. J. Bifurc. Chaos **14**, 1801–6 (2004). https://doi.org/10.1142/S0218127404010084

38. Litak, G., Kamin'ski, T., Rusinek, R., et al.: Patterns in the combustion process in a spark ignition engine. Chaos Solitons Fractals **35**, 578–585 (2008). https://doi.org/10.1016/j.chaos.2006.05.053

39. Litak, G., Kami'nski, T., Czarnigowski, J., Zukowski, D., Wendeker, M.: Cycle-to-cycle oscillations of heat release in a spark ignition engine. Meccanica **42**, 423–433 (2007). https://doi.org/10.1007/s11012-007-9066-6

40. Daw, C.S., Wagner, R.M., Edwards, K.D., Green, J.B.: Understanding the transition between conventional spark-ignited combustion and HCCI in a gasoline engine. Proc. Combust. Inst. **31**, 2887–2894 (2007). https://doi.org/10.1016/j.proci.2006.07.133

41. Yang, L.P., Song, E.Z., Ding, S.L., Brown, R.J., Marwan, N., Ma, X.Z.: Analysis of the dynamic characteristics of combustion instabilities in a pre-mixed lean-burn natural gas engine. Appl. Energy **183**, 746–759 (2016). https://doi.org/10.1016/j.apenergy.2016.09.037

42. Sen, A.K., Wang, J.H., Huang, Z.H.: Investigating the effect of hydrogen addition on cyclic variability in a natural gas spark ignition engine: wavelet multiresolution analysis. Appl. Energy **88**, 4860–6 (2011). https://doi.org/10.1016/j.apenergy.2011.06.030

43. Sen, A.K., Zheng, J.J., Huang, Z.H.: Dynamics of cycle-to-cycle variations in natural gas direct-injection spark-ignition. Appl. Energy **88**, 2324–34 (2011). https://doi.org/10.1016/j.apenergy.2011.01.009

44. Sen, A.K., Ash, S.K., Huang, B., Huang, Z.: Effect of exhaust gas recirculation on the cycle-to-cycle ariations in a natural gas spark ignition engine. Appl. Therm. Eng. **31**, 2247–2253 (2011). https://doi.org/10.1016/j.applthermaleng.2011.03.018

45. Li, G.X., Yao, B.F.: Nonlinear dynamics of cycle-to-cycle combustion variations in a lean-burn natural gas engine. Appl. Therm. Eng. **28**, 611–620 (2008). https://doi.org/10.1016/j.applthermaleng.2007.04.008

46. Letellier, C., Meunier-Guttin-Cluzel, S., Gouesbet, G., Neveu, F., Duverger, T., Cousyn, B.: Use of the nonlinear dynamical system theory to study cycle-to-cycle variations from spark-ignition engine pressure data. SAE paper no. 971640 (1997). https://doi.org/10.4271/971640

47. Sen, A.K., Litak, G., Yao, B.-F., Li, G.-X.: Analysis of pressure fluctuations in a natural gas engine under lean burn conditions. Appl. Therm. Eng. **30**, 776–779 (2010). https://doi.org/10.1016/j.applthermaleng.2009.11.002

48. Rocha-Martinez, J.A., Navarrete-Gonzales, T.D., Pavia-Miller, C.G., Paez-hernandez, R.: Otto and diesel engine models with cyclic variability. Revista Mexicana de Fisica **48**, 228–234 (2002)

49. Bogus, P., Merkisz, J.: Misfire detection of locomotive diesel engine by non-linear analysis. Mech. Syst. Signal Process. **19**, 881–889 (2005). https://doi.org/10.1016/j.ymssp.2004.06.004

50. Kabiraj, L., Sujith, R.I.: Nonlinear self-excited thermoacoustic oscillations: intermittency and flame blowout. J. Fluid Mech. **713**, 376–397 (2012). https://doi.org/10.1017/jfm.2012.463

51. Nair, V., Thampi, G., Sujith, R.I.: Engineering precursors to forewarn the onset of an impending combustion instability. In: Proceedings of the ASME Turbo Expo 2014: turbine

technical conference and exposition, 4B, V04BT04A005p (2014)

52. Nair, V., Sujith, R.I.: Intermittency as a transition state in combustor dynamics: an explanation for flame dynamics near lean blowout. Combust. Sci. Technol. **187**, 1821–1835 (2015). https://doi.org/10.1080/00102202.2015.1066339

53. Seshadri, A., Nair, V., Sujith, R.I.: A reduced-order deterministic model describing an intermittency route to combustion instability. Combust. Theor. Model. **20**, 1–16 (2016). https://doi.org/10.1080/13647830.2016.1143123

54. Sen, A.K., Longwic, R., Litak, G., Go'rski, K.: Analysis of cycle-to-cycle pressure oscillations in a diesel engine. Mech. Syst. Signal Process. **22**, 362–373 (2008). https://doi.org/10.1016/j.ymssp.2007.07.015

55. Yang, L.P., Ding, S.L., Litak, G., Song, E.Z., Ma, X.Z.: Identification and quantification analysis of non-linear dynamics properties of combustion instability in a diesel engine. Chaos **25**, 013105 (2015). https://doi.org/10.1063/1.4899056

56. Kyrtatos, P., Brückner, C., Boulouchos, K.: Cycle-to-cycle variations in diesel engines. Appl. Energy **171**, 120–132 (2016). https://doi.org/10.1016/j.apenergy.2016.03.015

57. Kennel, M.B., Brown, R., Abarbanel, H.D.I.: Determining embedding dimension for phase-space reconstruction using a geometrical construction. Phys. Rev. A **45**, 3403 (1992). https://doi.org/10.1103/PhysRevA.45.3403

58. Abarbanel, H.D.I.: Analysis of Observed Chaotic Data. Springer, New York (1996)

59. Eckmann, J.P., Kamphorst, S.O., Ruelle, D.: Recurrence plots of dynamical systems. EPL Europhys. Lett. **4**, 973–7 (1987)

60. Marwan, N., Romano, M.C., Thiel, M., Kurths, J.: Recurrence plots for the analysis of complex systems. Phys. Rep. **438**, 237–329 (2007). https://doi.org/10.1016/j.physrep.2006.11.001

61. Marwan, N., Wessel, N., Meyerfeldt, U., Schirdewan, A., Kurths, J.: Recurrence plot based measures of complexity and its application to heart rate variability data. Phys. Rev. E **66**, 026702 (2002). https://doi.org/10.1103/PhysRevE.66.026702

62. Mindlin, G.M., Gilmore, R.: Topological analysis and synthesis of chaotic time series. Physica D **58**, 229–242 (1992). https://doi.org/10.1016/0167-2789(92)90111-Y

63. Zbilut, J.P., Zaldívar-Comenges, J.M., Strozzi, F.: Recurrence quantification based Liapunov exponents for monitoring divergence in experimental data. Phys. Lett. A **297**, 173–181 (2002). https://doi.org/10.1016/S0375-9601(02)00436-X

64. Thiel, M., Romano, M.C., Kurths, J., Meucci, R., Allaria, E., Arecchi, F.T.: Influence of observational noise on the recurrence quantification analysis. Physica D **171**, 138–152 (2002). https://doi.org/10.1016/S0167-2789(02)00586-9

65. Schinkel, S., Dimigen, O., Marwan, N.: Selection of recurrence threshold for signal detection. Eur. Phys. J. Spec. Top. **164**, 45–53 (2008). https://doi.org/10.1140/epjst/e2008-00833-5

66. Bochner, S., Chandrasekharan, K.: Fourier Transforms. Princeton University Press, Princeton (1949)

67. Kaiser, G.: A Friendly Guide to Wavelets. Birkhaeuser, Boston (1994)

68. Ouahabi, A., Femmam, S.: Wavelet-based multifractal analysis of 1-D and 2-D signals: New results. Analog Integr Circ S **69**, 3–15 (2011). https://doi.org/10.1007/s10470-011-9620-y

69. Torrence, C., Compo, G.P.: A practical guide to wavelet analysis. Bull. Am. Meteorol. Soc. **79**(1), 61–78 (1998)

70. Sen, A.K., Litak, G., Taccani, R., Radu, R.: Wavelet analysis of cycle-to-cycle pressure variations in an internal combustion engine. Chaos Solitons Fractals **38**, 886–893 (2008). https://doi.org/10.1016/j.chaos.2007.01.041

71. Sen, A.K., Litak, G., Finney, C.E.A., Daw, C.S., Wagner, R.M.: Analysis of heat release dynamics in an internal combustion engine using multifractals and wavelets. Appl. Energy **87**, 1736–43 (2010). https://doi.org/10.1016/j.apenergy.2009.11.009

72. Farge, M.: Wavelet transforms and their applications to turbulence. Annu. Rev. Fluid Mech. **24**, 395–457 (1992)

73. Viggiano, A., Magi, V.: A comprehensive investigation on the emissions of ethanol HCCI engines. Appl. Energy **93**, 277–287 (2012). https://doi.org/10.1016/j.apenergy.2011.12.063

74. Saxena, S., Vuilleumier, D., Kozarac, D., Krieck, M., Dibble, R., Aceves, S.: Optimal operating conditions for wet ethanol in a HCCI engine using exhaust gas heat recovery. Appl. Energy **116**, 269–277 (2014). https://doi.org/10.1016/j.apenergy.2013.11.033

75. Heywood, J.B.: Internal Combustion Engine Fundamentals. McGraw-Hill, New York (1988).ntals